Application of a Novel, Non-doped, Organic Hole-transport Layer into Single-walled Carbon Nanotube/Silicon Heterojunction Solar Cells

Tom Grace[1], Hong Duc Pham[2], Christopher T. Gibson[1,3], Joseph G. Shapter[1,4] and Prashant Sonar [2,*]

[1] College of Science and Engineering, Flinders University, Bedford Park, SA, 5042, Australia; tom.grace@flinders.edu.au, christopher.gibson@flinders.edu.au, joe.shapter@flinders.edu.au.

[2] Institute of Future Environment and School of Chemistry, Physics and Mechanical Engineering, Queensland University of Technology (QUT), 2 George Street, Brisbane, QLD-4001, Australia; h22.pham@qut.edu.au, sonar.prashant@qut.edu.au.

[3] Flinders Institute for NanoScale Science and Technology, College of Science and Engineering, Flinders University, Bedford Park 5042, Australia; Flinders Microscopy and Microanalysis, College of Science and Engineering, Flinders University, Bedford Park 5042, Australia

[4] Australian Institute for Bioengineering and Nanotechnology, The University of Queensland, St Lucia Brisbane, Queensland 4072, Australia

***** Correspondence: sonar.prashant@qut.edu.au

Supplementary Material

The large area devices used in this work meant that to illuminate the entire cell active area, the light source had to be withdrawn from the cell such that the light intensity was 50 mW cm^{-2} as opposed to the more standard 100 mW cm^{-2} used for AM1.5 testing. This lower power was taken into account when calculating the PCE for these cells. Illumination was provided by a Newport 150 W Xenon lamp in a Newport arc lamp power supply model 69907. Lamp irradiation intensity was kept constant using a silicon reference device (PV Measurements, NIST-traceable calibration).

Solar Testing Lamp Spot Size Adjustments

Power Relationship

Two important aspects need to be considered when using the larger spot size. The first is how the PCE changes as a function of input light intensity. Under the 50 mW cm^{-2} source the current produced, and thus the Jsc of a cell will be less than under the full 100 mW cm^{-2} source. Ideally, by applying the reduced irradiation power in the PCE equation, the same PCE value would result at any input power. However, this is not the case. It has been seen from experimental observation that the PCE(%) of the silicon reference device (used to calibrate the light source in this thesis) drops as input power is lowered.

Figure S1 shows that, whilst the silicon reference cell displays the ideal linear trend of Jsc vs input power, the CNT/Si device does not. Furthermore, the PCE for the reference device decreases slightly over most of the plot before sharply dropping at low input powers. The opposite is true for the CNT/Si device where the PCE increases sharply from around 25% and lower. This is likely due to resistive power loss in the CNT film having a greater effect as the

film is required to transport greater currents. Thus, it can be seen that a more thorough investigation of the effect of changing input power is required to properly test large area CNT/Si devices.

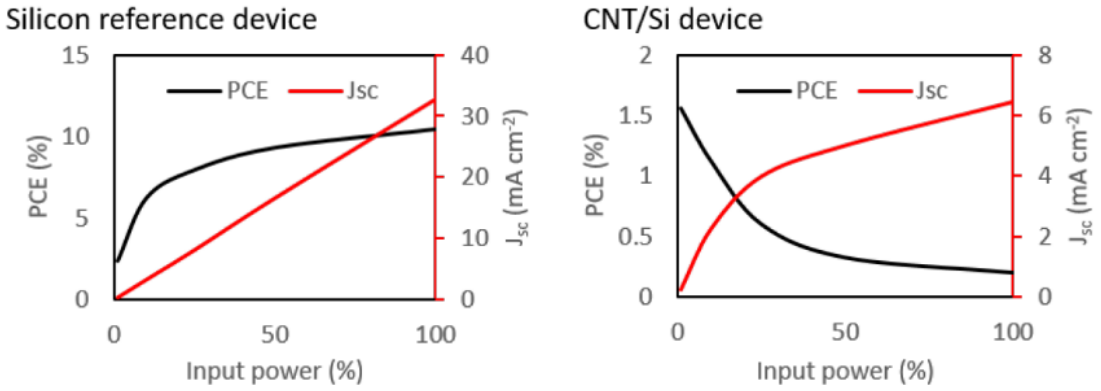

Figure S1. Effect of changing input power on photovoltaic properties in the silicon reference device and a CNT/Si device. The input power is a percentage of the optimal power of 100 mW cm^{-2}.

Lamp Spot Inhomogeneity

There is, however, another very important property of the light source that must be discussed. The power analysis assumes that the lamp power output does not vary across the lamp spot. For the very large area this is very unlikely to be the case and to image this inhomogeneity a thin aperture (approximately 1.5 mm by 9.5 mm) was placed over the silicon reference device and this aperture was moved from one outside edge of the light spot area to the other edge, with the current output recorded for each 1 mm step in both the horizontal and vertical directions. It was obvious that there is significant inhomogeneity present in the AM1.5 source used. The large area devices suffer a larger detrimental effect due to this intensity inhomogeneity as, a large area device positioned for maximum intensity (and thus maximum current output) will experience less irradiance, per unit area, compared to a small area device also positioned for maximum irradiance. This is because a large area device will be exposed to a greater proportion of the total light spot than a small area device.

In order to properly analyse this lamp spot area inhomogeneity, the silicon reference device was covered to leave only a 1 mm^2 aperture and was moved precisely across the large spot area both vertically and horizontally to image each square millimetre of the spot. The data produced from this experiment was plotted on a grid with μA values for each mm^2. The image, with colour gradient, makes it clear that the irradiance of the lamp spot is not consistent across the whole area. This analysis showed that a reading from reference device which implies an irradiance of 50 mW cm^{-2} from the AM1.5 source means the actual irradiance is 45 mW cm^{-2} for the large area cells.

The understanding of the power curve relationships and true light intensity meant that the correct PCE could be determined. The corrections were tested for a set of small area devices and directly compared with large device data. The %T of the CNT film was kept constant between these two sets as was the series of post fabrication treatments. Applying the scaling factor as determined from the 2D current map of the spot area yielded J_{sc} values much closer than the raw measurements.

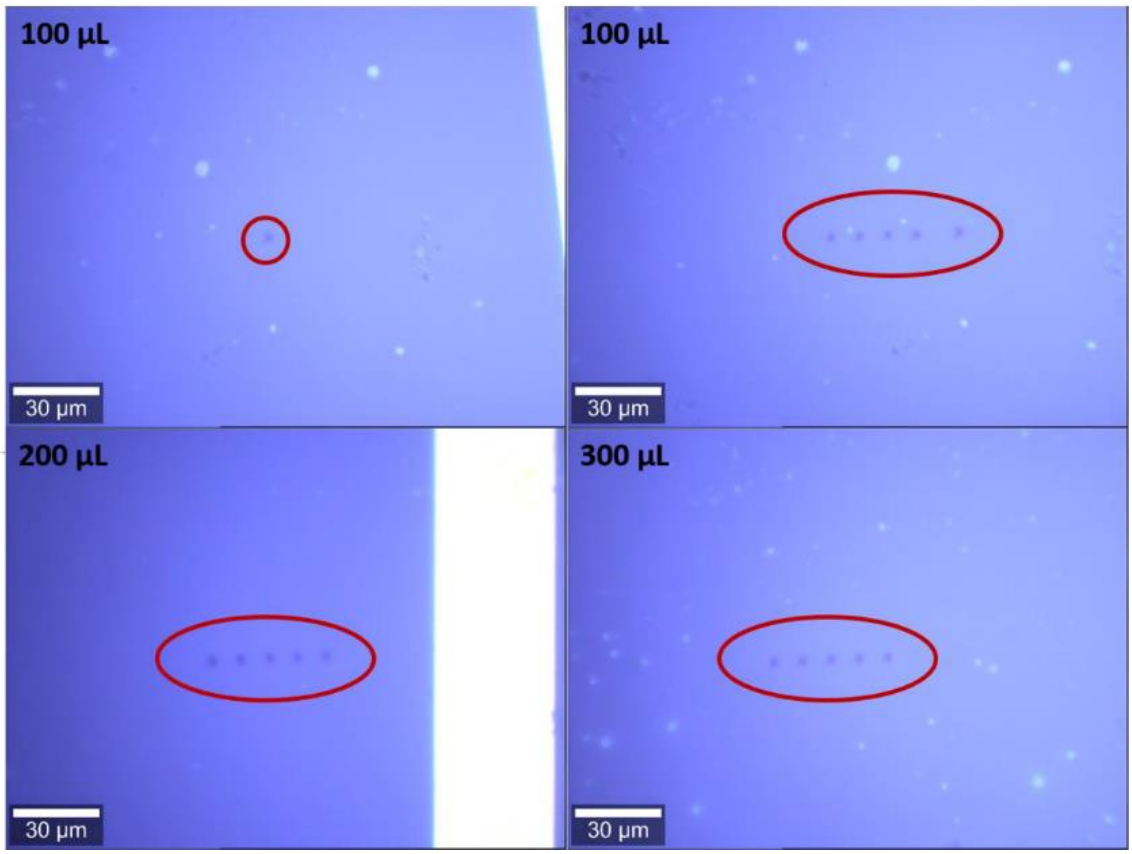

Figure S2. Optical microscope images of DAD films spun from different solution volumes. The blue areas are the DAD film, the large white areas are gold grid lines and the small white dots are air bubble holes in the film. The dark dots are burnt holes.

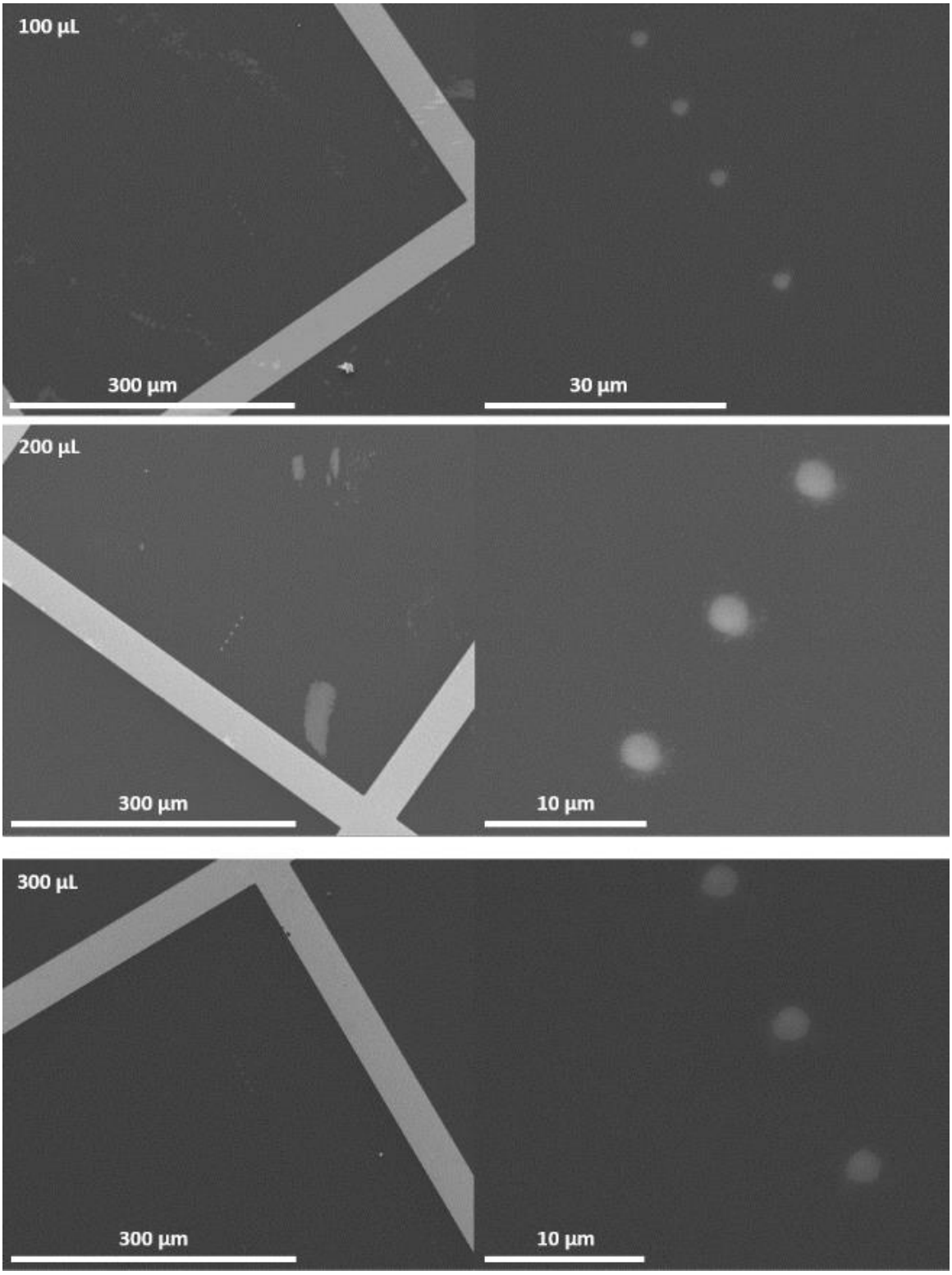

Figure S3. SEM images of DAD films spun from different solution volumes.

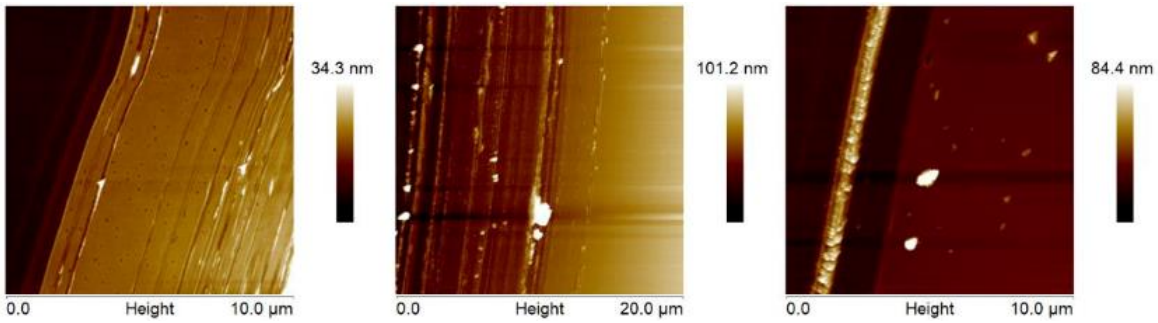

Figure S4. AFM height maps of DAD films spun from different solution volumes.

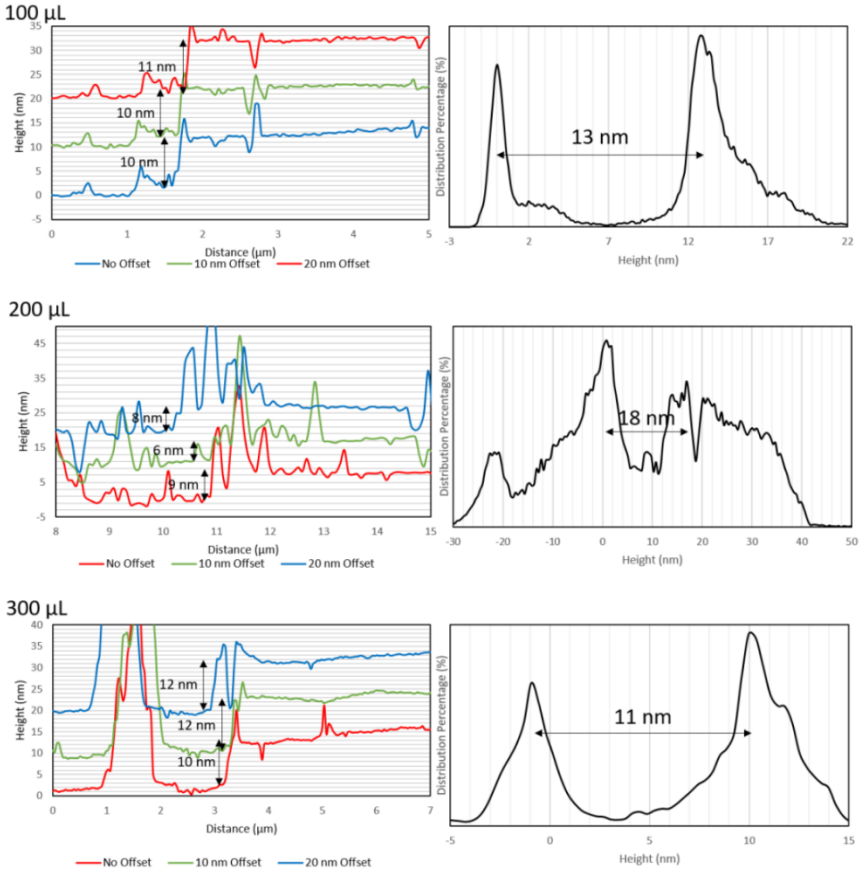

Figure S5. AFM cross sectional line graphs and percentage height distribution plots of DAD films spun from different solution volumes.

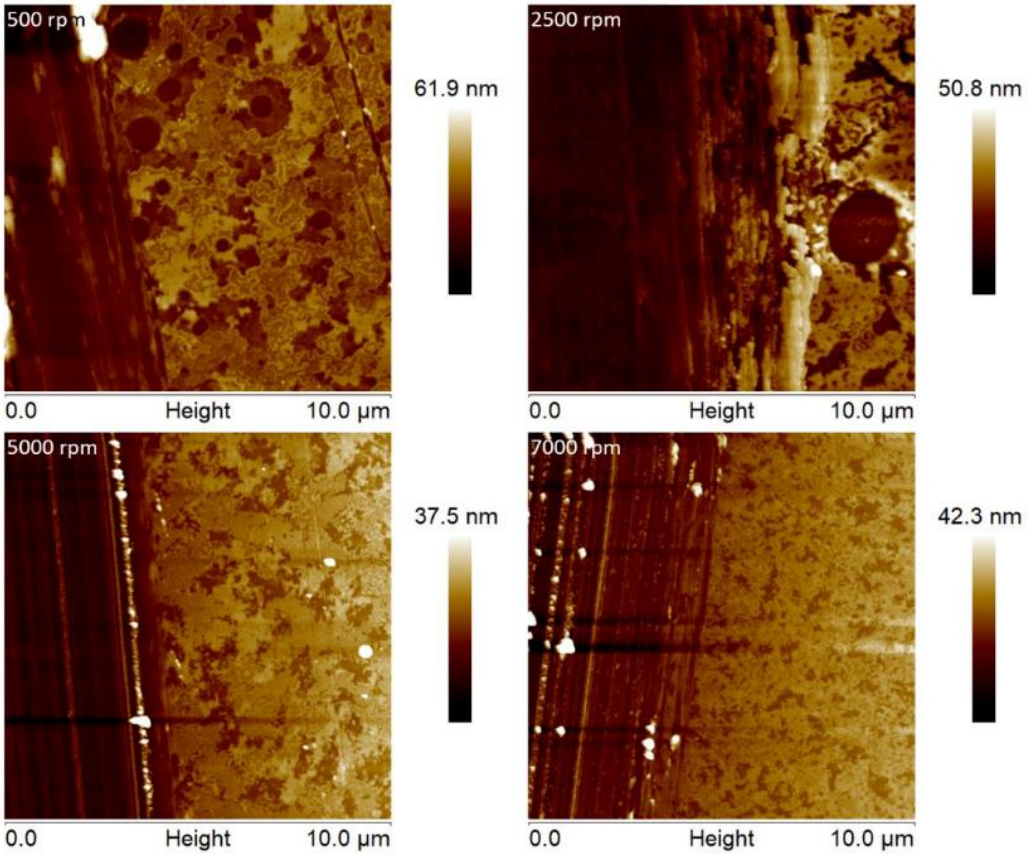

Figure S6. AFM height maps of DAD films spun at different speeds.

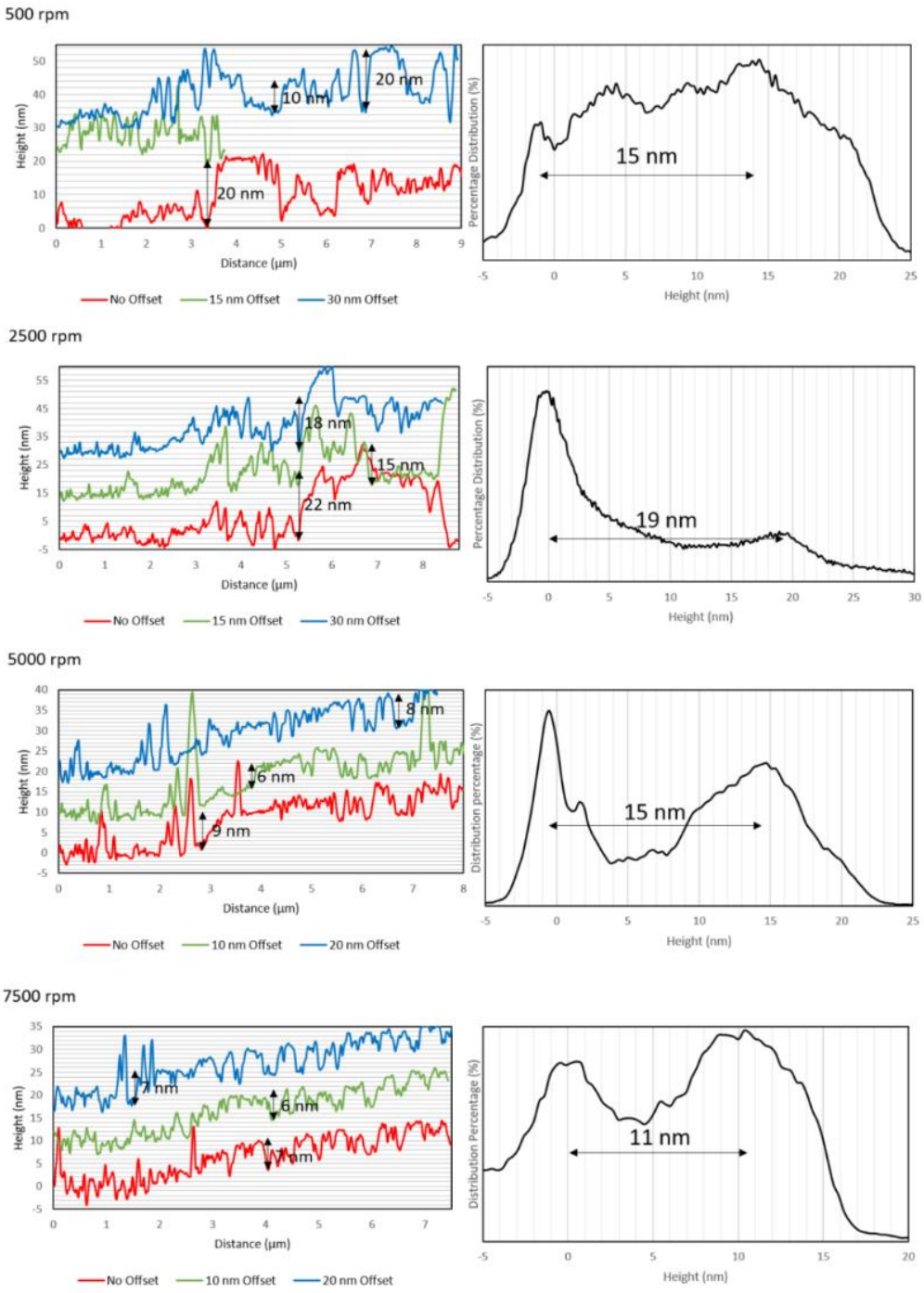

Figure S7. Cross-sectional line graphs and height distribution plots for DAD films spun at different spin speeds.

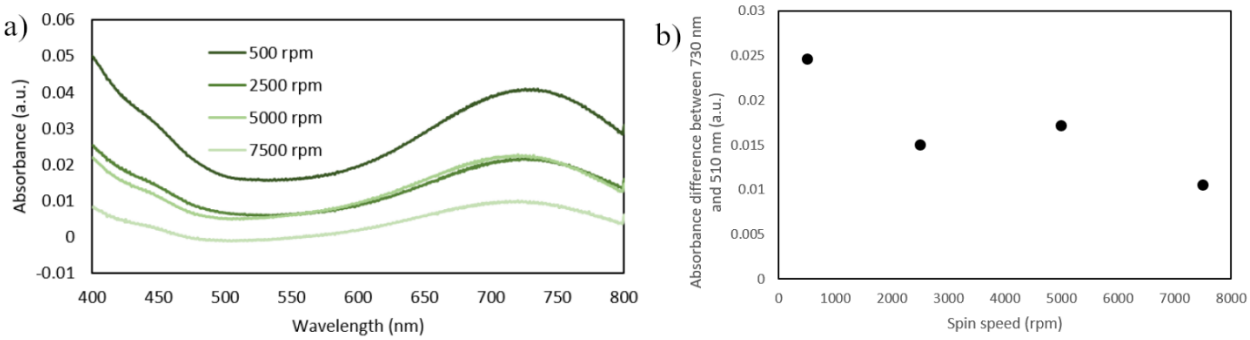

Figure S8. a) UV/Visible spectra of DAD films on glass spun from 200 µL aliquots dropwise for a variety of spin speeds. B) Peak-baseline absorbance difference vs spin speed of DAD films on glass.

The characteristic peak for DAD at roughly 730 nm decreases as the spin speed is increased, indicating that thinner films were produced at higher spin speeds. It is notable that there is no change in spectral shape between different spin speeds, indicating that the films were of the same structural composition, and just differed in volume of material on the surface. The corrected absorbance was plotted against spin speed showing the change in film thickness. Note that the fact that the 7500 rpm sample's spectrum dropped below an absorbance of 0 is due to the extremely low absorbance values recorded which will exacerbate any slight difference between the sample and the baseline glass slide.

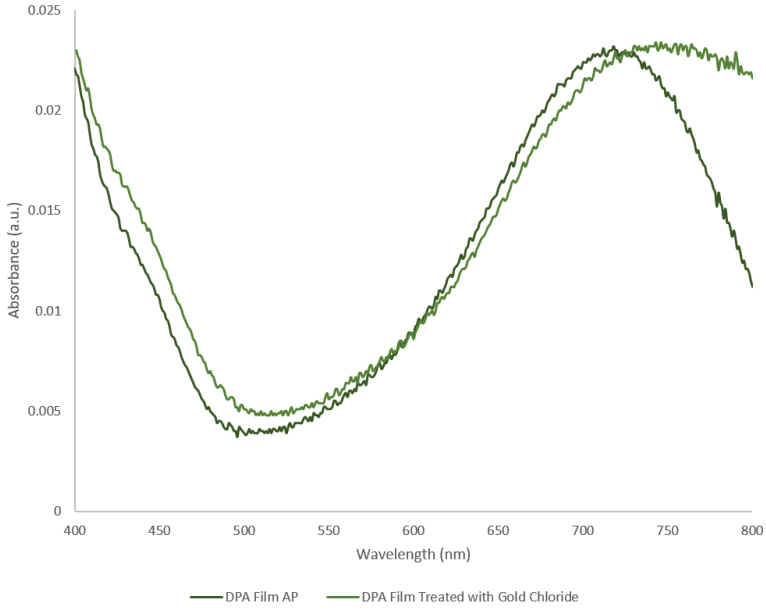

Figure S9. UV/Vis spectra of 2500 rpm DAD films on glass before and after exposure to $AuCl_3$ used in the devices for doping of the CNT layer.